

Blended Visual Binaries as Tests of Low Amplitude Orbit
Detection and Determination Capability in Long-Focus
Photographic Astrometry

Sarah Lee Lippincott and John L. Hershey
Sproul Observatory, Swarthmore College

Abstract

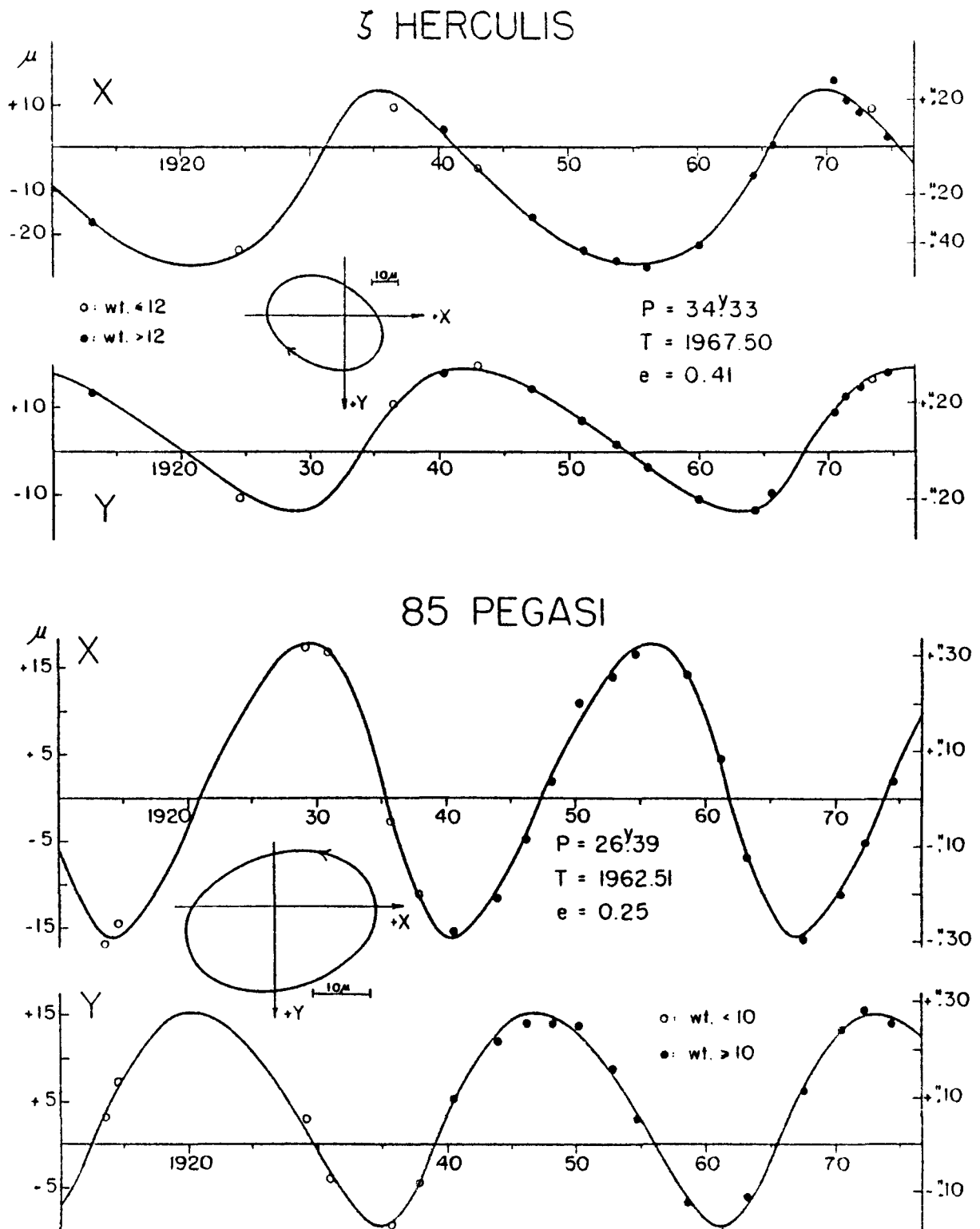
Photocentric orbital motions from 60-year Sproul plate series are shown for three visual binaries, ζ Her, 85 Peg and Ho 296. Mass ratios of the first two pairs, which have large-amplitude blended orbits, carry internal errors at the level of one percent. Orbital elements computed independently from the blended photographic observations agree closely with the well-determined visual orbits. Ho 296 serves as a test of the Sproul plate series to detect a 20-year orbit with an amplitude of two, or one, micron. Simulations of orbital motion in single star residual series confirm this detection capability, which corresponds to planetary mass for dark objects around nearby stars. A mass-luminosity diagram of the lower main sequence is shown, including one for invisible astrometric companions.

I. Introduction

The photographic study of double stars has two distinct aspects. For stellar pairs well resolved on the photographic plates, the relative motion can be determined. Most often the study is made from multiple exposure plates in the Hertz-sprung method, where a coarse grating is used to produce comparable images for two components of different magnitudes. Our concern here is with pairs or discovery of pairs which are completely unresolved on the photographic plate of a long-focus telescope. This occurs for separation of the components of approximately $1''.5$ or less. The unresolved image of the double is measured against a background of reference stars. Pairs with unequal masses and magnitudes can show a measurable photocentric orbit whose orbital elements can be determined similar to those in the relative orbit except for a diminution in the scale of the orbit. Elements in the relative orbit are generally determined from visual measurements taken from assorted telescopes with a number of different observers. This is especially true for long orbital periods which may extend to hundreds of years.

II. Techniques for Orbit Determination for Unresolved Binaries

The photographic observations from which orbital elements can be determined, on the other hand, can come from a single telescope representing a homogeneous set of data. Two examples of classical double stars are ζ Her and 85 Peg (Lippincott 1981); long interval series on each are measured for the first time on an electronic measuring machine. The computed displacement curves and the photocentric observations with π and μ removed are shown in Figures 1 and 2. These graphs are examples of the power of current photographic techniques; no new techniques can make 70 years elapse in any less time! With data extending back to 1914 with the Sproul refractor, almost two orbital periods are covered for ζ Her and more than two for 85 Peg, longer than any previous study. They result in values comparable in precision to the corresponding values in the relative orbit determined visually. Because the proper motion has to be determined, more than one complete period must be covered in the observations of a binary to fully separate the orbital period from the proper motion when the orbital elements are to be determined from the unresolved images. The coverage is less critical when the orbital elements are known from a visual



Figs. 1&2 PHOTOCENTRIC ORBITS DETERMINED AT SPROUL OBSERVATORY

Well-known naked eye visual binaries. Images on the Sproul photographs are unresolved and yield photocentric orbits. The computed displacement curves are from the measured positions. The photocentric orbital elements give values very close to the corresponding visual elements; the a , semimajor axis of the photocentric orbit for ζ Her is $0''.439$, and $0''.342$ for 85 Peg.

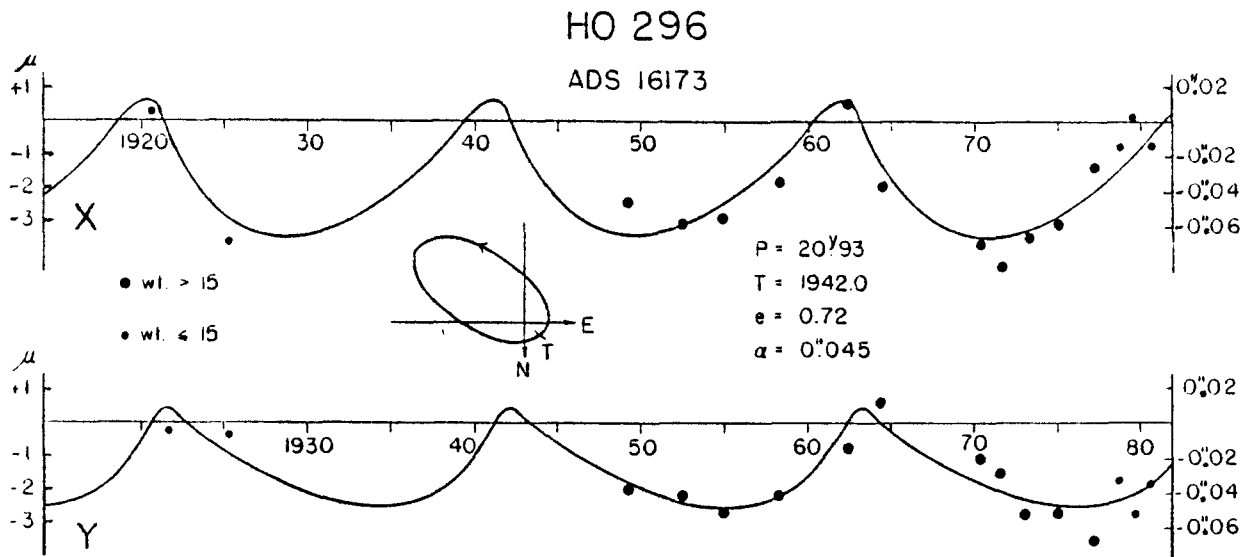


Fig. 3. Normal point positions in the photocentric orbit of the photographically blended visual binary Ho 296. The axis in each coordinate is the center of mass. The displacement curves result from adopting the elements of the visual orbit and solving for α , the photocentric semimajor axis. The inset is the two-dimensional photocentric orbit on the same scale as the separate displacement curves.

orbit and only the scale of the photocentric orbit is required as is the case for mass-ratio determinations. The scales of the ζ Her and 85 Peg orbits or their α , the semimajor axis of their photocentric orbits, are very large compared to the yearly mean errors of the observations, yielding mass ratios with errors at the level of 1%, assuming no error in β .

The case of Ho 296 (Hershey, 1981) is an example of an orbit with a far smaller value for α . Figure 3 shows a fit made by adopting the visual elements and solving for only the scale, α (and c_x , c_y , μ_x , μ_y). The agreement of the early points is especially good considering that the fit did not have the freedom to adjust P , e , T , i , ω and Ω . As with the first two cases, all of the orbital elements can be determined by automated computer program without prior knowledge from the visual orbit. The period determined from the photocentric positions agrees with that of the visual orbit to 3%, the periastron to 2%, and the eccentricity to 0.01 of the corresponding value determined visually. The agreement is notably good considering that the photocentric orbital half-amplitude is only two microns and the visual orbit is seven times larger.

III. Techniques and Level of Attainable Accuracy

The methods used to determine the orbital elements independently of the known relative orbit in the above examples are the same ones used to discover unseen companions of previously single stars and to analyze the orbital motion. Usually we estimate a P , T , and e from a graph of the normal point residuals in x and y , after a provisional least squares solution has removed c , π and μ . A computer program then accepts a range of values for P , T and e to determine the modified Thiele-Innes constants along with Δc and $\Delta \mu$ for each combination of P , T , and e desired. This "trial and error" method with attendant errors allows for a determination of

elements which represent the observations well. Subsequently a final least squares solution for c , μ , π and α , the scale of the photocentric orbit, is made. We have also the possibility of solving simultaneously for Δc_x , Δc_y , $\Delta \mu_x$, $\Delta \mu_y$, ΔP , ΔT , Δe , ΔA , ΔB , ΔF , ΔC , both separately in each coordinate and in combination of both coordinates for all constants. The errors for all eleven variables are calculated.

For short period orbital motion--that is, from $\sim \frac{1}{2}$ year up to ~ 4 years--the normal points may not readily reveal the orbit to visual inspection. A computer program has been designed to point out short periods with amplitudes near the noise level from the night mean residuals from a least squares solution for c , μ , and π . Various methods were explored for short period detection; many textbook methods presume data which are equally and continuously spaced in time. After some consultation on complex statistical methods, a simple procedure of trying a range period was adopted. The spacing of the periods is determined as a function of the period, and the length in time of the data set, so as not to change the phase by a large fraction at the end of the data range with each step in period. Amplitudes and their errors were computed for sinusoids by least squares solutions for each trial period. Astrometric observations are made during the same six or fewer months of each year. The annual missing segments in the data sometimes cause spurious amplitudes for periods near one year, one-half year, and two years. Orbital amplitudes of two or more times the error of unit weight would be apparent on inspection. Orbital amplitudes comparable to the error of unit weight are detectable by the program. As the amplitude goes below the error of unit weight the detection capability rapidly weakens.

Ho 296 may serve as a "laboratory test" of the telescope to detect a 2 micron perturbation as found in the above analysis. Since the visual orbit is known very accurately and independently of the photographic observations, part of the computed orbital displacement can be removed, leaving the random and systematic errors of the telescope unaffected, but with reduced orbital information. With one-half the amplitude removed, an automated differential correction solution was able to converge on all elements of a one-micron orbit. The period differed by 5% from the visual orbit, the periastron by 2% of the period, and the eccentricity by 0.2. This resulted from 30 years of continuous but not highly intensive coverage. The result corresponds to a detectability of a 5-8 Jupiter mass object around a late-type main sequence star at 5 parsecs.

In order to further test the accuracy of graphical and computer search for orbital motion with one micron for the semimajor axis, orbital displacements have been added into normal point residuals of apparently single stars. Three star series (Wolf 294, Grb 1618, Ross 128: Hershey et al. 1980) were chosen with varying observational coverage since 1937, comparable to the average of stars nearer than 5 parsecs. For example, the Wolf 294 series extends from 1937-1979; the normal points have an average integrated exposure time of a half hour assuming the current basic exposure time. An orbit with 16.6 yr period (that of Ross 614) and one with 2.45 yr (that of Wolf 1962) were used, scaled to $\alpha = 1\mu$. ($1\mu = 0''.019$ with the Sproul refractor.) The orientation on the plane of the sky is such that the amplitudes are about equal in x and y . A significant eccentricity leads to a definition of T and further refines the aspects of the displacements to be analyzed. Inspection of the adjusted normal point residuals indicated something more than random motion. A provisional period and periastron passage could be estimated within a certain range for the long period motion. Various values around the estimated P , T , and e were used in the computer programs described earlier. For the cases of

the applied short period, i.e., $P = 2.45$ yr, the short-period detection program was used with a follow-up of the trial and error program with a range of $\frac{1}{2}$ year for the period surrounding the one suggested by the previous program. Various values of T and e were used. The significant values for mass determination are those of P and α . For the examples above, the long period determined ranged from 16.8 to 17.2 and for the short period the trial and error analysis converged to $P = 2.4$ yr. The α 's determined from the long and short period ranged from 0.90μ to 1.4μ .

With this detection capability as an example, we can extrapolate for various distances and adopted masses of the primary to see the ranges of masses of unseen companions which can be discovered. Figure 4 shows what mass objects can be found with $\alpha = 1\mu$ and $P = 40$ yr, with the masses as a function of parallax and mass of the visible component. We see that masses lower than 10 times Jupiter's mass ($0.01M_{\odot}$) are detectable. With an observational interval ≥ 4 decades, we can find systems with longer orbital periods which facilitate the detection of increasingly smaller companion masses. Thus, objects of ten times Jupiter's mass are detectable for stars out to 20 parsecs. Observational data with the coverage and accuracy of the Sproul data described above for the majority of the stars within 5 parsecs should be able to reveal unseen companions close to the level of a Jupiter mass with periods 20 yr and up.

IV. The Mass-Luminosity Relation: Mass Ratios, Masses and Unseen Companions

The lower end of the mass luminosity relation, mostly determined with current techniques discussed above, is shown in Figure 5, where the luminosity is given as M_V . For the cases of binary systems with one component unseen, the mass of the primary is estimated from its absolute magnitude, and the secondary mass and mag. are

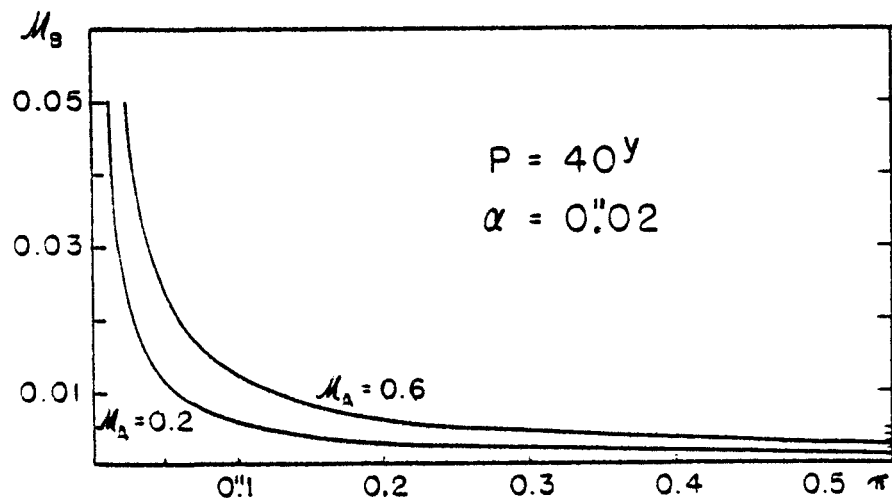


Fig. 4. Expected $M_{B\odot}$ at various distances of an unresolved binary with $M_{A\odot}$ of $0.2 M_{\odot}$ and $0.6 M_{\odot}$ for $P = 40$ yr and $\alpha = 1\mu$.

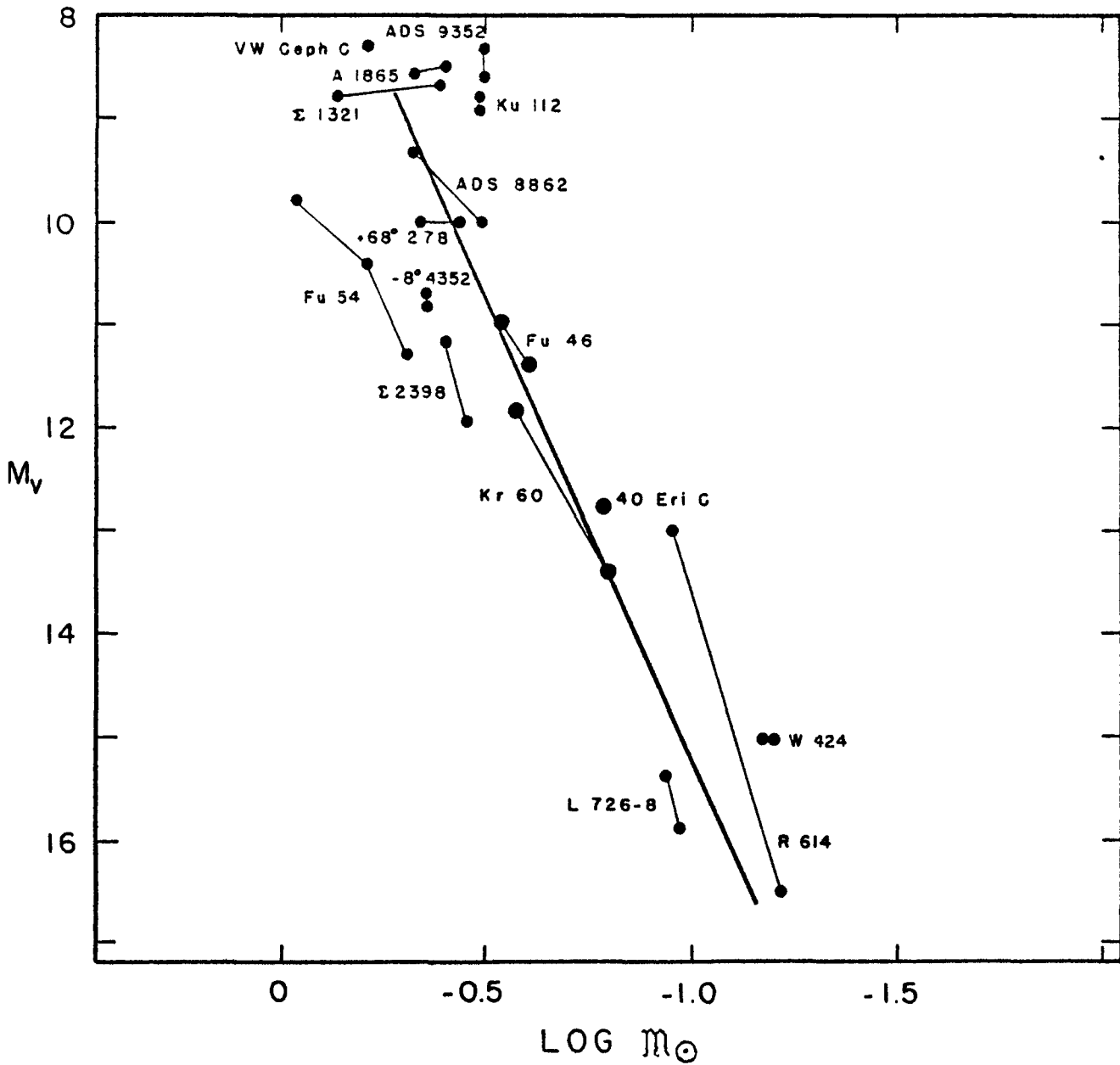


Fig. 5. Mass-luminosity diagram for stars at the faint end of the Main Sequence.

chosen from a likely combination following from the relation:

$$\alpha^3 P^{-2} = (B-\beta)^3 (M_A + M_B);$$

when \$M_B\$ is small compared to \$M_A\$, i.e., \$(M_A + M_B) \sim M_A\$, and the \$\Delta m\$ large, then

$$M_B = \alpha P^{-2/3} M_A^{2/3}.$$

The \$\alpha\$ is the semimajor axis of the photocentric orbit in astronomical units;

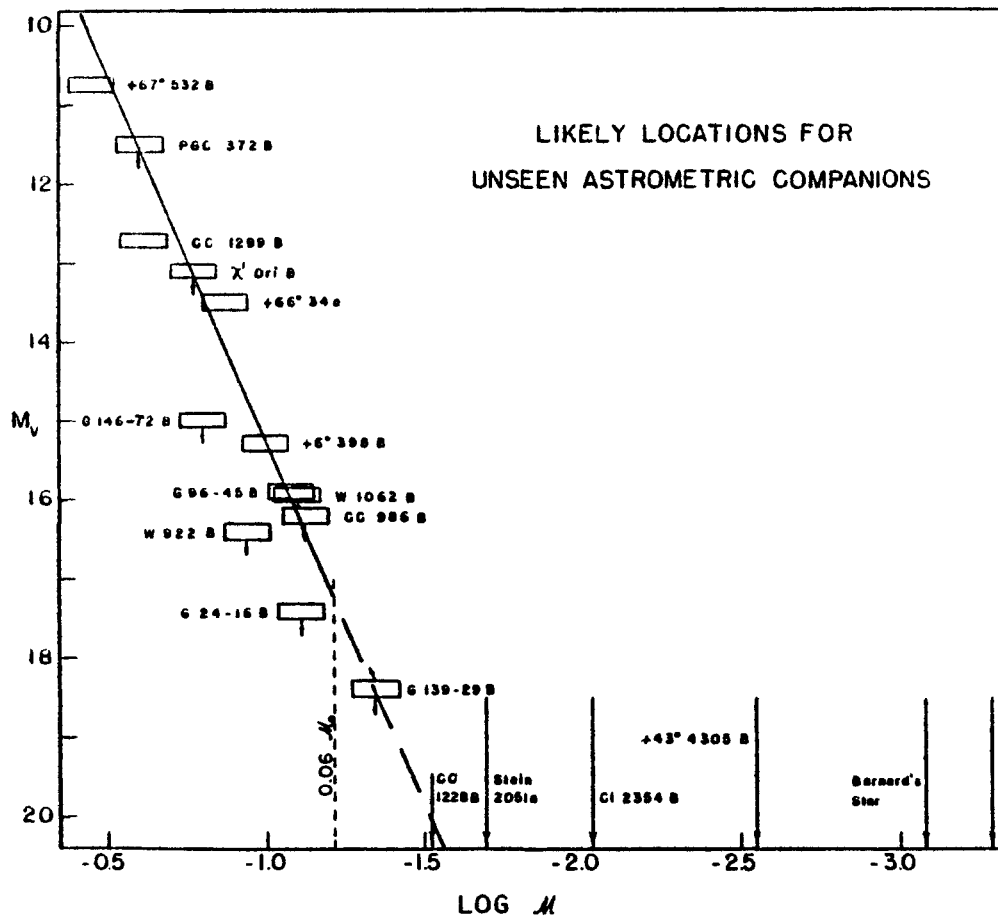


Fig. 6. Likely locations for unseen astrometric companions assuming locations on the mass-luminosity relation of the primary appropriate to M_V and spectrum.

β is a function of the Δm . Thus an extension of the M-L relation is made for the unseen companions and is shown in Figure 6. The horizontal extension gives an indication of the uncertainties in the mass, and the vertical line indicates the direction of uncertainty in the M_V . A fuller discussion of the faint end of mass luminosity relation will appear elsewhere.

The support of the National Science Foundation through grant AST 80-17320 and past grants in all aspects of this work is gratefully acknowledged.

References

- Hershey, J. L. 1981. Submitted to A.J.
 Hershey, J. L., Borgman, E. R., and Worth, M. D. 1980. *Ap. J.* **240**, 130.
 Lippincott, S. L. 1981. *P.A.S.P.* **93**, June.

DISCUSSION

HERSHEY: Did you give an accuracy for those mass ratios?

LIPPINCOTT: The mass ratio accuracy is way down, at about a hundredth, if you assume that the delta-m's are accurate and that the "a" coming from the visual orbit has no error. Again, a plea for good delta-m's for all of these stars!